

SIMULATING FUTURE GPS CLOCK SCENARIOS WITH TWO COMPOSITE CLOCK ALGORITHMS

Matthias Suess
German Aerospace Centre (DLR)
Oberpfaffenhofen, Germany
Matthias.suess@dlr.de

Demetrios Matsakis
United States Naval Observatory (USNO)
Washington, D.C., USA
Demetrios.Matsakis@usno.navy.mil

Charles A. Greenhall
Jet Propulsion Laboratory, California Institute of Technology
Pasadena, CA, USA
cgreenhall@jpl.nasa.gov

Abstract

Using the GPS Toolkit, the GPS constellation is simulated using 31 satellites (SV) and a ground network of 17 monitor stations (MS). At every 15-minute measurement epoch, the monitor stations measure the time signals of all satellites above a parameterized elevation angle. Once a day, the satellite clock estimates are uploaded to the satellites. Two composite clock algorithms are applied to estimate the station and satellite clocks. The first composite clock (B) is based on the Brown algorithm [1], and is now used by GPS. The second one (G) is based on the Greenhall algorithm [2]. The composite clock of G and B performances are investigated using three ground-clock models. Model C simulates the current GPS configuration, in which all stations are equipped with cesium clocks, except for masers at USNO and Alternate Master Clock (AMC) sites. Model M is an improved situation in which every station is equipped with active hydrogen masers. Finally, Models F and O are future scenarios in which the USNO and AMC stations are equipped with fountain clocks instead of masers. Model F is a rubidium fountain, while Model O is a more precise but futuristic Optical Fountain. Each model is evaluated using three performance metrics. The timing-related user range error having all satellites available is the first performance index (PI1). The second performance index (PI2) relates to the stability of the broadcast GPS system time itself. The third performance index (PI3) evaluates the stability of the time scales computed by the two composite clocks. A distinction is made between the "Signal-in-Space" accuracy and that available through a GNSS receiver.

INTRODUCTION

In the beginning, the GPS control segment consisted of five monitor stations, including one master control station at Schriever, Air Force Base (AFB). Today, the data from 12 additional control stations operated by the National Geospatial-Intelligence Agency (NGA) are integrated to the GPS control segment (Figure 1) [1,2]. Thus, a total of 17 monitor stations are available.

Now, the monitor stations at USNO, Washington DC, and Schriever AFB are referenced to masers, while all other stations are equipped with HP 5071 cesium clocks [3]. USNO is planning to replace the maser references in Washington and Schriever with rubidium fountains. The paper uses a simplified model of the operational GPS Kalman Filter, limited to clock estimates, to investigate by simulation the impact of improved monitor station clocks on the GPS timing performance.

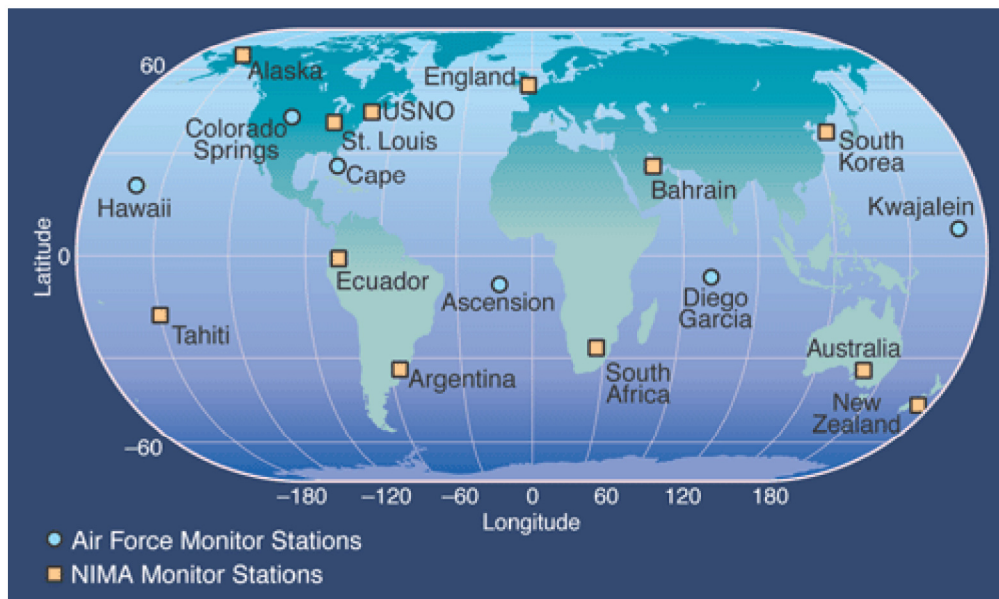


Figure 1. GPS ground segment

(<http://www.aerospace.org/publications/crosslink/summer2002/04.html>).

SIMULATION OF THE GPS WORKFLOW

Using the GPS toolkit software [4], the positions of 31 satellites were modelled based on the GPS almanac file of week 531. The satellites are equipped with Rubidium Atomic Frequency Standards (RAFS). Each monitor station observes the time offset, compared to its reference clock, of the satellites in view. The measurements are simulated with a 15-minute spacing, a white Gaussian noise of 0.7 ns (1 sigma), and an elevation angle mask of 20°. The measurement noise models pseudorange measurements, which provide time information, but are approximately 100 times noisier than carrier-phase data.

The clock parameters computed by the Kalman Filter are uploaded to each satellite once a day as a broadcast model. In this simulation, we assume the update occurs when the satellite is in view over Schriever and the clock broadcast parameters are older than 1 day.

For this work, only clock parameters are solved for. In the operational filter, satellite orbit and other parameters are simultaneously included and the correlations among the full set of parameters would be expected to decrease the precision of the derived solutions. This would most likely decrease the differences we have computed between the clock models. However, double-differencing between satellite and station pairs allows one to solve for all other parameters without estimating clocks, and to solve for clocks in a second solution using the non-clock parameters as inputs.

SIMULATION OF THREE IMPROVED MONITOR STATION CLOCKS AND SATELLITE CLOCKS

Each clock is modelled with a three-state vector $X(t)$, which is their phase, frequency, and drift offset [5,6]. It is modelled by the stochastic differential equation (SDE)

$$\frac{dX}{dt}(t) = \begin{pmatrix} 0 & 1 & 0 \\ 0 & 0 & 1 \\ 0 & 0 & 0 \end{pmatrix} X(t) + W(t)$$

$$EW(t)W^T(t) = \begin{pmatrix} q_1 & 0 & 0 \\ 0 & q_2 & 0 \\ 0 & 0 & q_3 \end{pmatrix} = Q(0s)$$

with a deterministic zero start value: $X(t_0)=0$.

The three q 's measure the noise contributions from white frequency modulation (WFM), random walk frequency modulation (RWFM), and random run frequency modulation (RRFM). Neglecting some terms [6], the q 's can be related to the Allan and Hadamard deviations as:

$$ADEV^2(\tau) = q_1\tau^{-1} + \frac{1}{3}q_2\tau + \frac{1}{20}q_3\tau^3 + \dots$$

$$HDEV^2(\tau) = q_1\tau^{-1} + \frac{1}{6}q_2\tau + \frac{11}{120}q_3\tau^3 + \dots$$

The discrete solution of the SDE, with τ equal to 15 min, is used to simulate the clock types [6-8]. Following the assumptions of the Kalman Filter, it can be shown that the process noise matrix $Q(\tau)$ is a simple function of the q 's and the filter time spacing τ :

$$Q(\tau) = \begin{pmatrix} q_1\tau + q_2\frac{1}{3}\tau^3 + q_3\frac{1}{20}\tau^5 & q_2\frac{1}{2}\tau^2 + q_3\frac{1}{8}\tau^4 & q_3\frac{1}{6}\tau^3 \\ q_2\frac{1}{2}\tau^2 + q_3\frac{1}{8}\tau^4 & q_2\tau + q_3\frac{1}{3}\tau^3 & q_3\frac{1}{2}\tau^2 \\ q_3\frac{1}{6}\tau^3 & q_3\frac{1}{2}\tau^2 & q_3\tau \end{pmatrix}.$$

Three different types of monitor station clocks are simulated: cesium, active hydrogen maser (AHM), and fountain clocks. Their stochastic components (q's) together with the RAFS are specified in Table 1, and typical Allan deviations are shown in Figure 2. The values for these q's should not be taken as authoritative by any means, nor should the associated Allan deviations be assumed as anything but a rough approximation of the clocks.

Table 1. Clock noise models.

	q₁ WFM [s²/ s]	q₂ RWFM [s²/ s³]	q₃ RRFM [s²/ s⁵]
Cesium	2.50e-23	4.44e-37	5e-53
AHM	2.8e-26	1.1e-35	4.4e-51
Fountain	2.5e-26	1.1e-37	1.1e-55
Optical Ftn	4.4e-27	1.1e-37	1.1e-55
RAFS	1.0e-24	1.1e-35	2.8e-46

Since the data are assumed to be processed in 15-minute batches, the printed values are scaled by factor of 900 from the rounded-off values used to generate the time series.

For numerical issues it is found to be useful to change the units of the q values (Table 1), which are conventionally given in seconds by seconds, to nanoseconds by day:

$$\left(\frac{10^{18}}{86400^{-1}} q_1 \quad \frac{10^{18}}{86400^{-3}} q_2 \quad \frac{10^{18}}{86400^{-5}} q_3 \right) \left[\frac{ns^2}{d} \quad \frac{ns^2}{d^3} \quad \frac{ns^2}{d^5} \right].$$

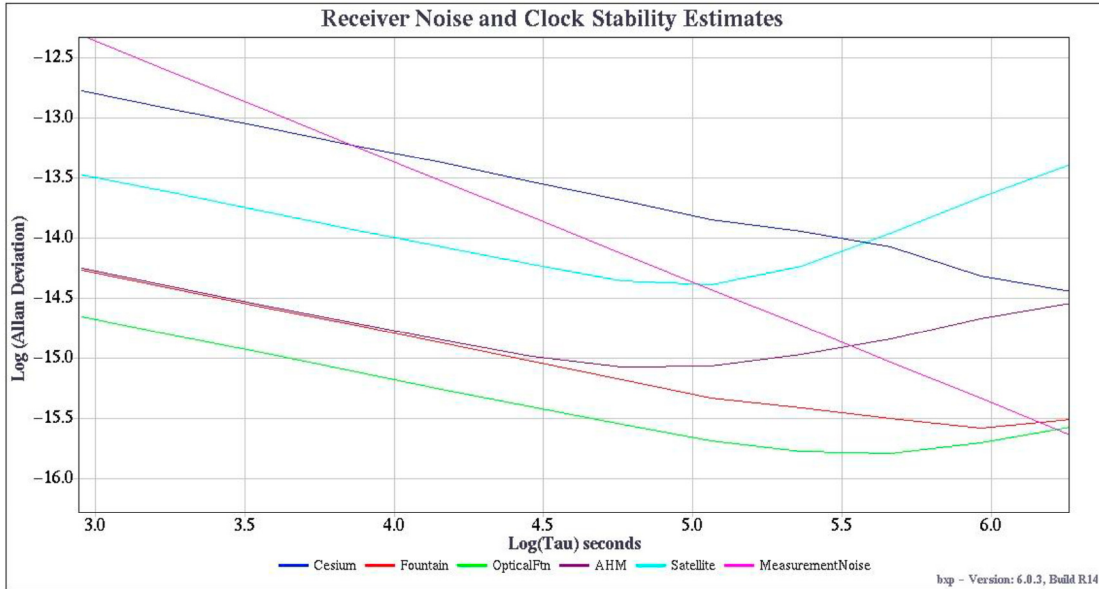


Figure 2. Allan deviation of one individual clock simulation of each modelled type. (It is assumed that the necessary resources are expended to keep the masers and the optical fountains within their environmental specifications, and that the receiver’s white phase pseudorange noise is diluted by eight independent simultaneous satellite measurements)

COMPOSITE CLOCK ALGORITHMS – BROWN AND GREENHALL

Two composite clock algorithms [7,8] are applied to process the time offset measurements between the control stations and the satellite clocks and to estimate the three states of the satellite and control station clocks with respect to its implicitly defined time scales. Since N clocks involve maximal N-1 linearly independent measurements, each composite clock algorithm includes a method to prevent the formal covariance of the solution parameters from growing without bound. The covariance reductions further obscure intuitive understanding of the solutions, but protects against computer limitations in handling large numbers.

THE BROWN COMPOSITE CLOCK

It can be shown [7] that no measured quantity is affected if the Kalman Filter covariance estimates $C(t)$ are reduced at each iteration step as follows:

$$B(C(t)) = C(t) - \bar{H}(\bar{H}^T C^{-1}(t) \bar{H})^{-1} \bar{H}^T$$

with

$$\bar{H} = \begin{pmatrix} I_3 \\ \vdots \\ I_3 \end{pmatrix} \in R^{3N \times 3}$$

Sorting the covariance by the states more clearly illustrates the operation of the Brown reduction. Each of the nine $N \times N$ sub matrix C_{ij} with $i, j \in \{x, y, d\}$ is subtracted by a $N \times N$ matrix with a common element defined by c_{ij}

$$C = \begin{pmatrix} C_{xx} & C_{xy} & C_{xd} \\ C_{yx} & C_{yy} & C_{yd} \\ C_{dx} & C_{dy} & C_{dd} \end{pmatrix} \rightarrow B(C) = \begin{pmatrix} C_{xx} & C_{xy} & C_{xd} \\ C_{yx} & C_{yy} & C_{yd} \\ C_{dx} & C_{dy} & C_{dd} \end{pmatrix} - \begin{pmatrix} 1_{N,N} c_{xx} & 1_{N,N} c_{xy} & 1_{N,N} c_{xd} \\ 1_{N,N} c_{yx} & 1_{N,N} c_{yy} & 1_{N,N} c_{yd} \\ 1_{N,N} c_{dx} & 1_{N,N} c_{dy} & 1_{N,N} c_{dd} \end{pmatrix}$$

with

$$(\bar{H}^T C^{-1}(t) \bar{H})^{-1} = \begin{pmatrix} c_{xx} & c_{xy} & c_{xd} \\ c_{yx} & c_{yy} & c_{yd} \\ c_{dx} & c_{dy} & c_{dd} \end{pmatrix} \text{ and } 1_{N,N} = \begin{pmatrix} 1 & \dots & 1 \\ \vdots & & \vdots \\ 1 & \dots & 1 \end{pmatrix} \in R^{N \times N}.$$

As a test of the programming, we have computed solutions with and without the covariance reduction, and verified that all quantities seen by the user are indeed unchanged. The Kalman filter is executed every 15 minutes and, after every iteration of the Kalman filter, the Brown reduction is applied. It results a series of reduced covariances which are called:

$$C_B(t_k) = B(F(C_B(t_{k-1})))$$

with the matrix function F models the Kalman filter iteration. The initial values are

$$\hat{X}(t_0) = 0 \text{ and } C_B(t_0) = 1e^{10} Q(\tau).$$

THE GREENHALL COMPOSITE CLOCK

The reduction method by Greenhall is of a similar manner; however, it works on the sub matrix C_{xx} of the phase states [8]. Using the auxiliary matrix

$$S = \begin{pmatrix} A & 0 & 0 \\ 0 & I_N & 0 \\ 0 & 0 & I_N \end{pmatrix}$$

with

$$A = (I_N - 1_N 1_N^T (1_N^T C_{xx}^{-1} 1_N)^{-1}) \text{ and } 1_N = \begin{pmatrix} 1 \\ \vdots \\ 1 \end{pmatrix} \in R^N$$

the Greenhall reduction is defined by

$$G(C(t)) = SC(t)S^T.$$

The matrix operation only affects the sub-matrixes involving the phase-parts:

$$C = \begin{pmatrix} C_{xx} & C_{xy} & C_{xd} \\ C_{yx} & * & * \\ C_{dx} & * & * \end{pmatrix} \rightarrow G(C) = \begin{pmatrix} C_{xx}^* & AC_{xy} & AC_{xd} \\ C_{xy}A^T & * & * \\ C_{xd}A^T & * & * \end{pmatrix}$$

with

$$C_{xx}^* = C_{xx} - \mathbf{1}_N (\mathbf{1}_N^T C_{xx}^{-1} \mathbf{1}_N)^{-1} \mathbf{1}_N^T.$$

As pointed out by Greenhall [8], running the Kalman filter with his reduction method changes the phase estimates, but not the frequency and drift estimates. The reduced covariance of the Greenhall composite clock is defined by:

$$C_G(t_k) = G(F(C_G(t_{k-1}))).$$

The same initial values as in case of Brown are used.

Using the Kalman filter with the Brown reduction is called the Brown composite clock, whereas running the Kalman filter with the Greenhall reduction is called the Greenhall composite clock.

THREE GROUND SEGMENT MODELS

Table 2 outlines three different ground segment models for the stability of the monitor station clocks.

Table 2. Model definition.

Model C	Cesium at every station except for AHMs at Schriever and USNO
Model M	AHMs at every station
Model F	Cesiums at every station except at Schriever and USNO, where USNO will maintain rubidium-based atomic fountains
Model O	As in Model F, except that the “optical fountains” have a factor of 2.4 less WFM noise

Model C describes the current situation in GPS, Model F represents the rubidium atomic fountains which the USNO is planning to install at its two facilities in the rather near future, and the other models represent possible future scenarios.

PERFORMANCE INDICES 1, 2, AND 3

In order to assess the different models three performance indices (PI) are defined. The following nomenclature is used

$$X = (x \ y \ d)^T, \quad \hat{X} = (\hat{x} \ \hat{y} \ \hat{d})^T \quad \text{and} \quad \tilde{X} = X - \hat{X}$$

with $x, y, d \in R^N$ the phase, frequency, and drift simulations and $\hat{x}, \hat{y}, \hat{d} \in R^N$ the corresponding estimates.

PI1: THE TIME-RELATED USER RANGE ERROR

The first index measures the accuracy of the clock broadcast models (BM), which are the latest uploads of their three-state Kalman filter estimates. For each satellite k, the broadcast model is updated at least every 24 hours and consists of three parameters used by the users to correct the clock:

$$BM_k(t) = a_0 + a_1(t - t_{upload}) + \frac{1}{2}a_2(t - t_{upload})^2,$$

where the step-function time-dependence of the model parameters (a_0, a_1, a_2) has been suppressed.

For each phase value $x_k(t)$ of satellite clock k at time t, the phase estimation error in this correction is given by

$$\tilde{x}_{BM,k}(t) = x_k(t) - BM_k(t).$$

The PI1 is defined by the root mean square error of the time series of empirical standard deviation of the corrected satellite clocks:

$$PI1 = \sqrt{\frac{1}{l} \sum_i \sigma^2(\{\tilde{x}_k(t_i)|k\})}$$

where l is the number of time samples.

PI1 is understandable as the average asynchronization of the broadcast model-corrected clocks at time t. It is a measure of the signal-in-space limitations to real-time positioning or synchronization with GPS. In order to allow the clock parameter determinations to mature (become independent of initial assumptions), PI1 (and PI2), are computed excluding the first day's data.

PI2: THE STABILITY OF THE BROADCASTED GPS SATELLITE TIME

The second performance index, PI2, evaluates the stability of the average GPS satellite time as broadcast:

$$PI2(\tau) = ADEV\left(\frac{1}{31} \sum_{k=1}^{31} \tilde{x}_{BM,k}(t), \tau\right).$$

Again, this represents the signal-in-space performance, undisturbed by other error effects (see PI1).

PI3: THE TIME SCALE STABILITY

Both composite clocks define its time scales within the Kalman filter. In the case of the Greenhall composite clock, the time scale weights are given by

$$w_G(t) = C_{G,xx}^{-1}(t) \mathbf{1}_N (\mathbf{1}_N^T C_{G,xx}^{-1}(t) \mathbf{1}_N)^{-1}$$

with

$$C_G(t) = \begin{pmatrix} C_{G,xx}(t) & C_{G,xy}(t) & C_{G,xd}(t) \\ C_{G,yx}(t) & C_{G,yy}(t) & C_{G,yd}(t) \\ C_{G,dx}(t) & C_{G,dy}(t) & C_{G,dd}(t) \end{pmatrix}$$

and its time scale is

$$sys_G(t) = w_G^T(t) \tilde{x}(t).$$

In contrast, the time scale of the Brown composite clock is the phase of the implicit ensemble mean. Using the Brown weight of all states

$$w_B^T(t) = ((\bar{H}^T C_B^{-1}(t) \bar{H})^{-1} \bar{H}^T C_B^{-1}(t)) (\mathbf{1}, :),$$

it is defined by

$$sys_B(t) = w_B^T(t) \begin{pmatrix} \tilde{x}(t) \\ \tilde{y}(t) \\ \tilde{d}(t) \end{pmatrix}.$$

The Brown time scale includes the corrected frequency and drift estimates as well. The third performance index, PI3, assesses the stability of GPS Time as computed within the two composite clocks.

$$PI3(\tau, sys_{\bullet}(t)) = ADEV(sys_{\bullet}(t), \tau)$$

Assuming the time t is large enough for the parameters to fully mature, PI3 is stationary and given by the Allan deviation of the system time.

For comparison reasons, the tau-weighted ADEV [9] is defined as:

$$ADEV_{\tau\text{-weighted}}^2(\tau) = \sum_{k=1}^N w_k^2(\tau) ADEV_k^2(\tau)$$

with weights

$$w_k(\tau) = \left(\sum_{i=1}^N \frac{1}{ADEV_i^2(\tau)} \right)^{-1} \frac{1}{ADEV_k^2(\tau)}$$

and $ADEV_k(\tau)$ the theoretical Allan deviation of clock k based on their q-values.

EVALUATION OF THREE MODELS

Each model is simulated with both composite clocks over a time period of 80 days, which correspond to around 7680 samples, and the three performance indices are calculated.

PERFORMANCE INDEX 1 AND 2

Figure 3 shows very little difference between the models in PI1, which is a measure of GPS's real-time signal-in-space performance. This is expected because any improvements in the predictive ability by the ground clocks should be masked by the individual satellite clocks' stochastic variations over the 24 hours between uploads. The Greenhall composite clock lightly outperforms Brown's for all models, although the difference would be masked by the user's receiver noise.

Similar results are shown in Figures 4 and 5, which is how PI2 would be computed by a worldwide array of noiseless receivers that did not have direct access to the GPS ground clocks and could only observe satellite broadcasts.

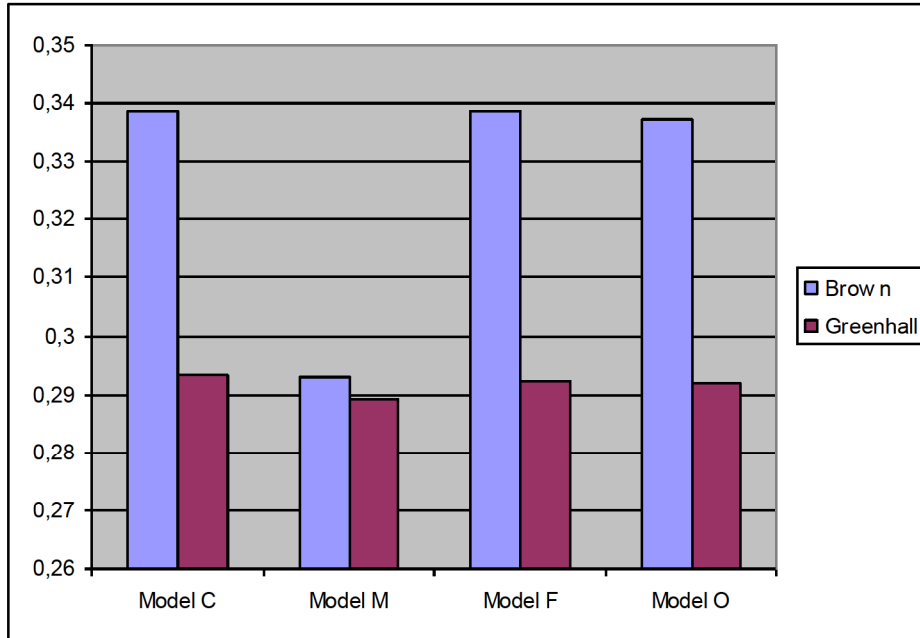


Figure 3. Signal-in-space comparison of the PII for the three scenarios and the two composite clocks (as would be observed with a noiseless GPS receiver). The actual performance as seen by a user would be a convolution of the plotted PII with the measurement noise, dilution of precision, multipath errors, etc.

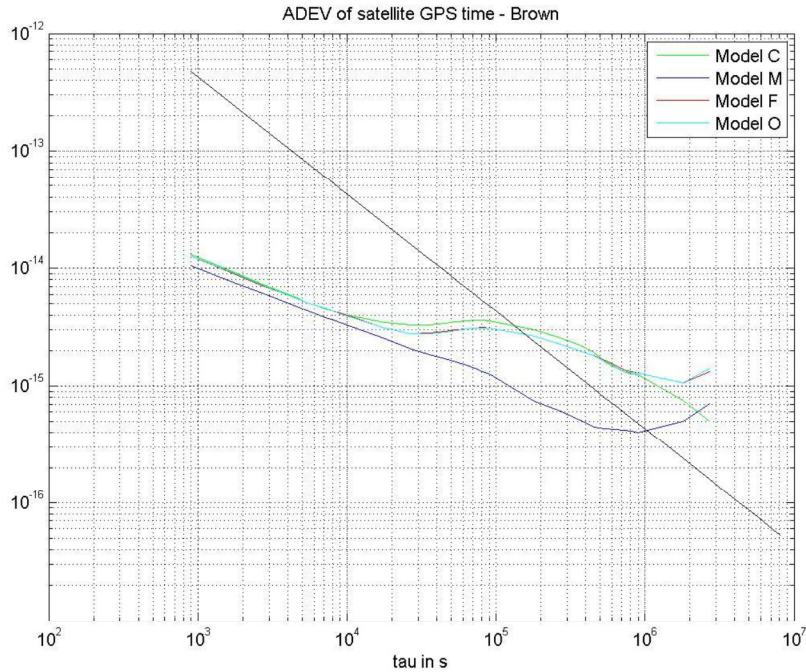


Figure 4. PI2 using Brown composite clock and a noiseless GPS receiver. The straight line with slope $1/\tau$ is an estimate of the masking effects of 700 ps of pseudorange noise and eight satellites simultaneously in view; but a carrier-phase-enabled receiver's noise limitation would be roughly two orders of magnitude lower for the shortest averaging time, and somewhat better than $1.E-15$ at 1 day.

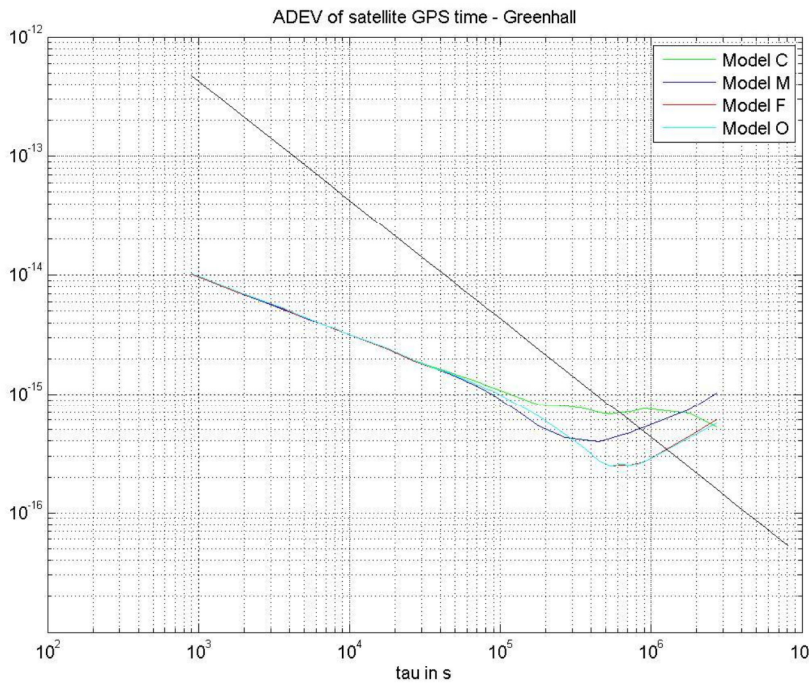


Figure 5. PI2 using Greenhall composite clock and a noiseless GPS receiver. The masking effect of pseudorange-only measurements is estimated as in the previous figure.

PERFORMANCE INDEX 3

Figure 6 compares the Allan deviations of the Brown and Greenhall time scales for each model. For both composite clocks, the stability improves for all models compared to Model C.

In the case of Brown and averaging times shorter than 1 day, the model M is the most promising one, model O and F fall on top of each other and model C is around two times worse than models F/O. The Brown composite clock does not fully make use of the improved model F/O. For averaging times longer than 1 day, the RWFm part of the AHM decreases the performance of the model M. The other ones show more or less a WFM behavior which results from the cesium clocks.

In the case of Greenhall and averaging times shorter than 1 day, models M and O as well as models F and C fall on top of each other. Since the model parameters for atomic fountains result in one “optical fountain” (model O) are roughly as stable as the RSS stability of an average of five masers for averaging times smaller than 1 day, it is also not surprising that, in a 17-station solution, Models M and O are roughly equivalent and also more stable than Model C. Since the WFM amount of a AHM and an atomic fountain are close to each other, it explains the performance similarity of the models F and C. For averaging times longer than 1 day, the solution for models O and F are more stable than that of models M and C.

The Greenhall time scale is more stable than the Brown time scale for any model for averaging times shorter than 1 day.

The PI3 values given in Figure 6 show that use of better ground clocks would result in GPS Time being more stable with regard to UTC. We note that actual GPS Time is stabilized through steering to UTC (USNO). This steering becomes significant on the scale of a few days, and is ignored here. It also follows that the stability of GPS Time itself is only relevant to the extent it minimizes the amount of steering applied to GPS Time. Even though GPS Time is intended for navigational purposes only and users interested in UTC should apply the corrections broadcast in subframe 4 page 18 of the GPS Navigation message to derive UTC (USNO) directly, we can assume that the stability of GPS Time will translate into the stability of GPS’s delivered prediction of UTC (USNO).

Another and closely related effect of improved PI3 would be to decrease the required steering of GPS Time and the uncertainty in the broadcast corrections for UTC (USNO), although receiver noise will be a limiting factor here.

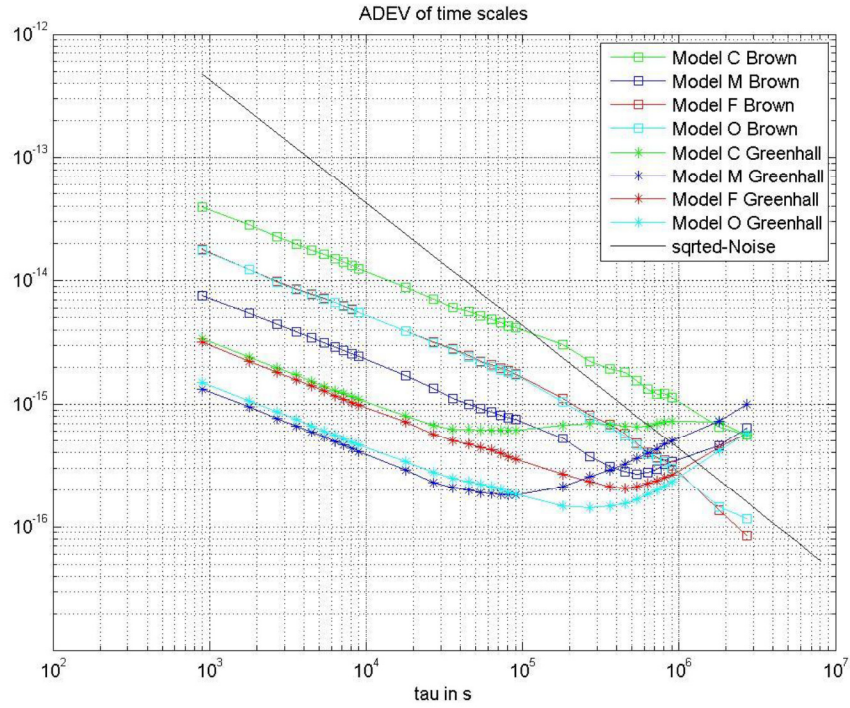


Figure 6. PI3 of the four models and the two composite clocks. The masking effect of pseudorange-only measurements is estimated as in the previous figures.

Figures 7, 8, 9, and 10 compare the two time scales, the tau-weighted ADEV, and the participating clock ADEVs for each model. In the case of model C (Figure 7), the Greenhall time scale and the tau-weighted ADEV are close to each other for averaging times smaller than 1 day and more stable than the most stable clock of the ensemble, the AHM. The Brown stability (squares) violates this condition and most likely follows the average of the cesium clocks (upper solid line).

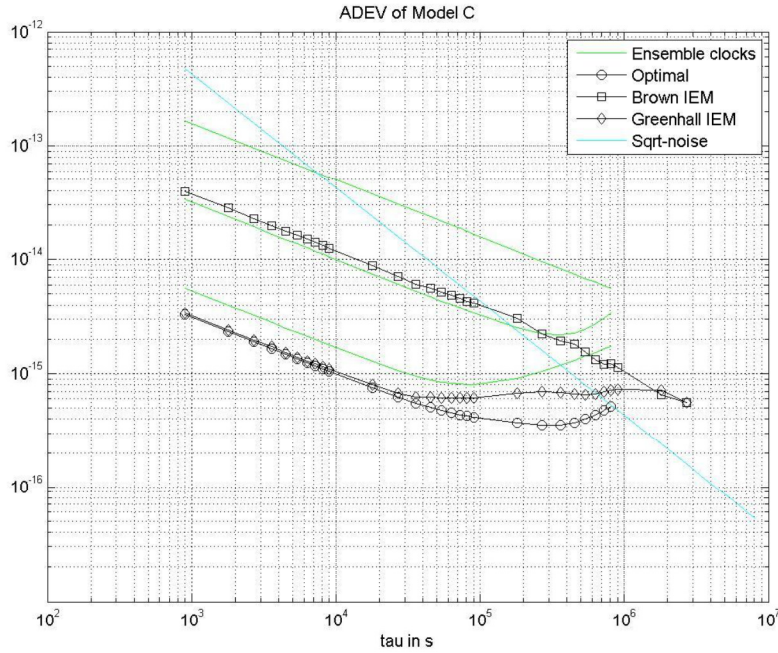


Figure 7. Comparison of ensemble clocks of model C and time scales. The masking effect of pseudorange-only measurements is estimated as in the previous figures.

In the case of model M (Figure 8), the tau-weighted ADEV and the Greenhall time scale are close to each other and, again, more stable than the most stable ensemble clock (AHM). The Brown time scale is less stable than the AHM for averaging times shorter than 1 day. It looks like that the Brown time scale follows the average stability of the RAFS.

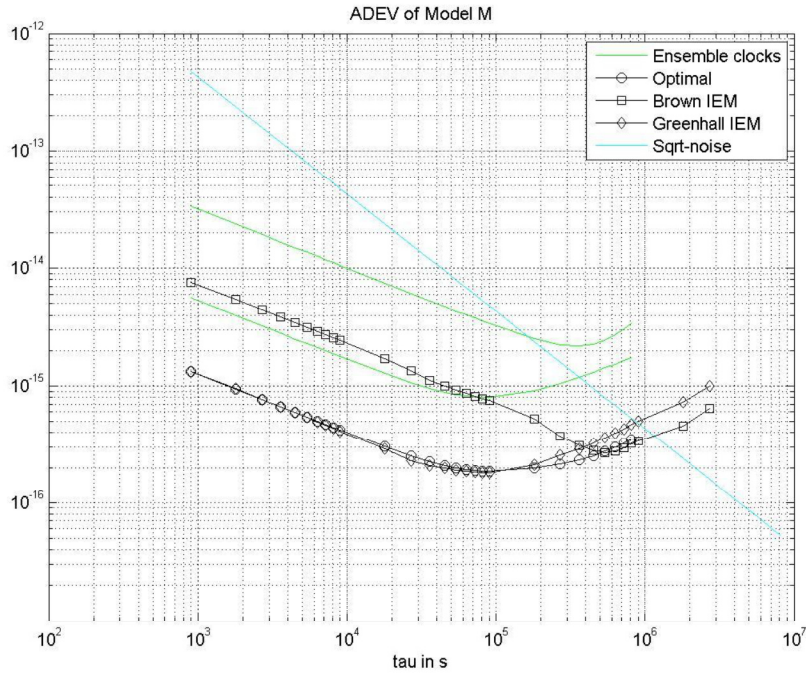


Figure 8. Comparison of ensemble clocks of model M and time scales. . The masking effect of pseudorange-only measurements is estimated as in the previous figure.

In the case of Model F (Figure 9), the tau-weighted ADEV and the Greenhall times scale are close to each other and are more stable than the most stable clock for every averaging time. This condition is violated by the Brown time scale.

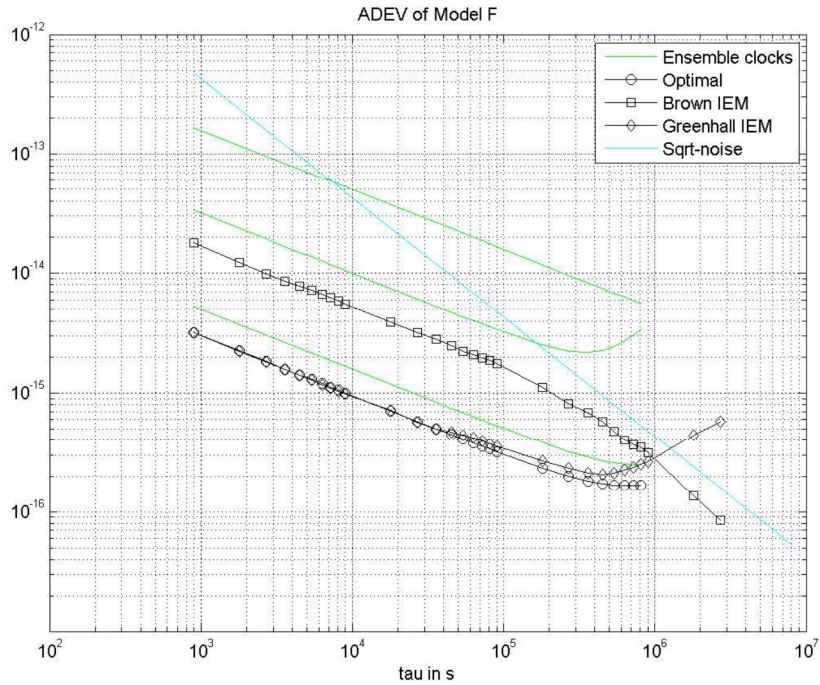


Figure 9. Comparison of ensemble clocks of model F and time scales. The masking effect of pseudorange-only measurements is estimated as in the previous figures.

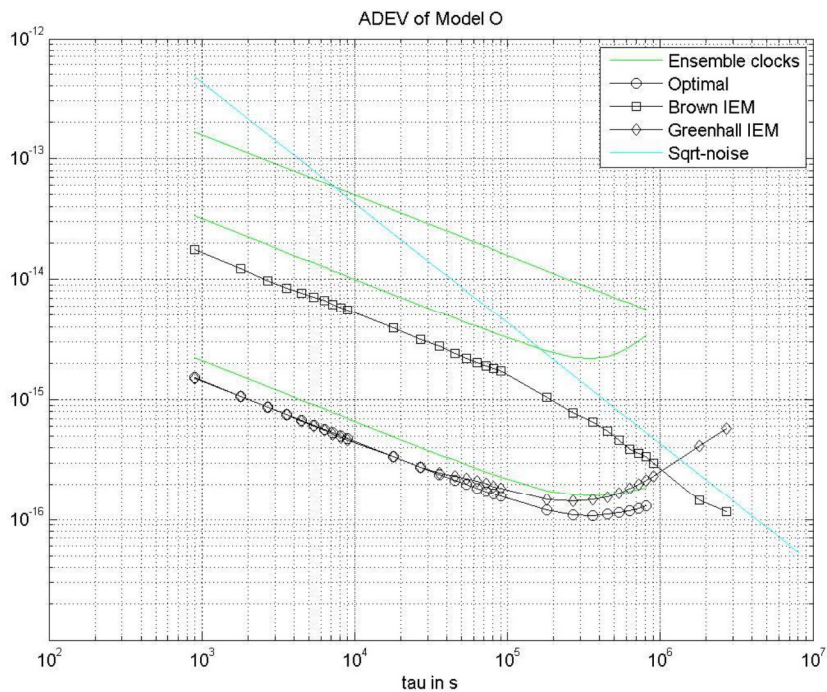


Figure 10. Comparison of ensemble clocks of model O and time scales. The masking effect of pseudorange-only measurements is estimated as in the previous figures.

Again, the tau-weighted ADEV and the Greenhall times scale are close to each other and are more stable than the most stable clock for every averaging time for model O. The Brown time scale violates this condition.

In the above discussion, the significance of measurement noise has not been directly addressed. The Kalman filter's response to the measurement noise is to downweight the innovations (new data). Without carrier-phase data, satellite clocks are unobservable for $\tau < 1.E04$ seconds, while Optical Fountains are modelled as being quieter to $\tau = 10$ days. Therefore, the derived timescale deviations stem from the smoothing aspect of the Kaman Filter. An ideal clock noiseless measured against a GPS monitor site clock would observe the computed Allan deviation against the timescale-corrected monitor site clock, provided the assumptions of the model remained valid. That same ideal clock's data would measure a similar Allan deviation against the uncorrected monitor clock if the differences were simply smoothed, although the 17 monitor site clocks would not then be on the same basis. On the other hand, for the overwhelming number of users accessing the timescale with a GPS receiver, timing will be limited by the measurement noise to the region above the line with slope $1/\tau$ in Figures 5 through 10.

IMPACT OF MEASUREMENT NOISE AND MIS-TUNING OF Q VALUES

Although measurement noise directly masks the low-tau performance of the timescale from the user, and heavily smoothes the data, the final result remains valid in a properly modelled situation. The results are not valid in the unmodelled case of sudden clock variations or failures below any outlier rejection threshold, and this would distort the position and time-determination of the GPS user.

Confining ourselves to the parameters and constraints of the Gaussian modelling, Figure 11 shows the impact of ten times more and less measurement noise on the performance index P11. Since the impact is similar for all models, model O is chosen as an example. The figure shows the quotient between the nominal P11 and the test P11. Obviously, more measurement noise decreases the performance around 50%, whereas less measurement noise barely helps. The impact is similar for both composite clocks.

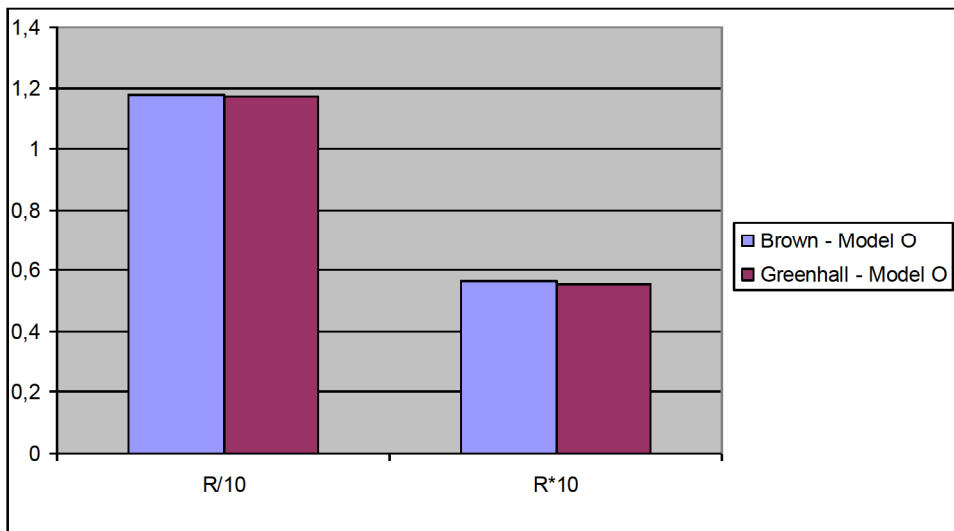


Figure 11. Impact of R variations on P11 of model O.

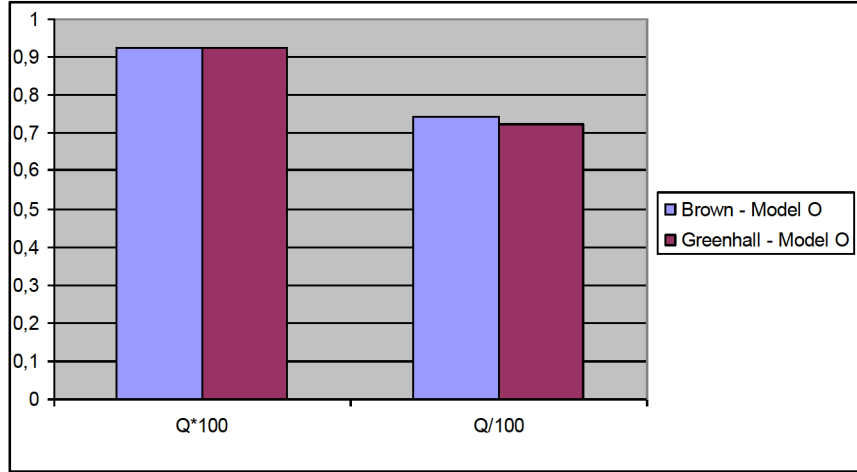


Figure 12. Impact of Q mis-modelling on PII of model O.

Figure 12 shows the impact of mis-modelling the Q values on PII. Two cases are simulated: the first one applies a 100 times higher and the second a 100 times smaller Q value. We note that the clock simulations are not changed and are based on the right Q. The quotient of the nominal PII and the test PII decreases in both cases; thus, the performance decreases. This is an indication that the Kalman filter is tuned right. This is the case for both composite clocks.

COMBINATION OF GREENHALL AND BROWN REDUCTION

Both reduction methods generate a time series of covariance matrices and estimates. An empirical study was performed which investigates the impact on the estimates and covariances of combining both methods. The two combinations are:

$$B(G(F(C_{B(G)}(t_{k-1})))) = C_{B(G)}(t_k) \text{ and } G(B(F(C_{G(B)}(t_{k-1})))) = C_{G(B)}(t_k).$$

The simulations point out that:

- Both combinations compute the same estimates as just using the Greenhall reduction

$$\hat{X}_{B(G)}(t_k) = \hat{X}_{G(B)}(t_k) = \hat{X}_G(t_k).$$

- The operations commute and compute the same covariance

$$C_{B(G)}(t_k) = C_{G(B)}(t_k).$$

The benefit of the combination is that also the frequency and drift parts of the Greenhall covariance are reduced by the Brown reduction. This is illustrated by Figure 13. The upper plot shows the frequency covariance of clock 1 using the Greenhall reduction. Obviously, the frequency covariance is not reduced. Figure 14 shows the effect of combining Brown and Greenhall. Clearly, the covariance is reduced.

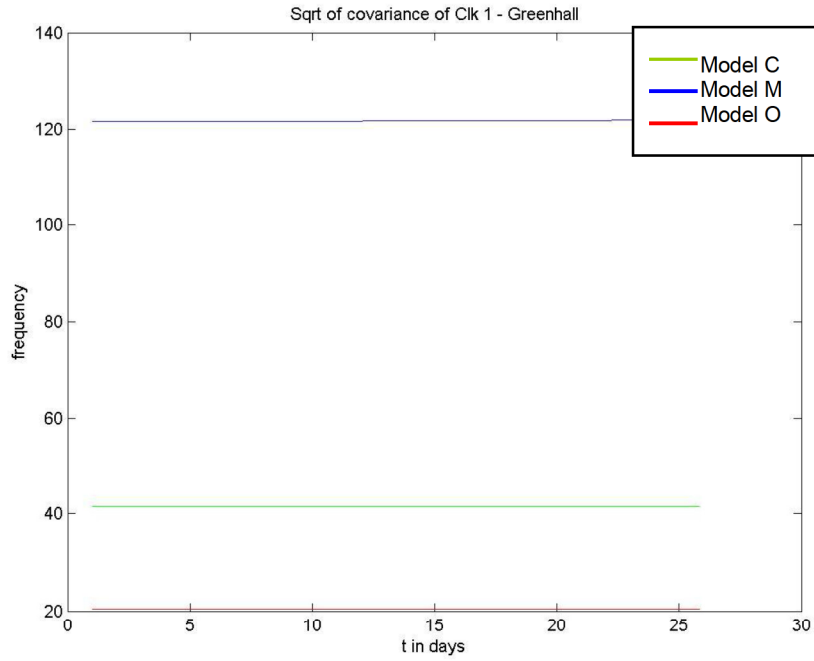


Figure 13. Greenhall frequency covariance of clock 1, in units of ns/d.

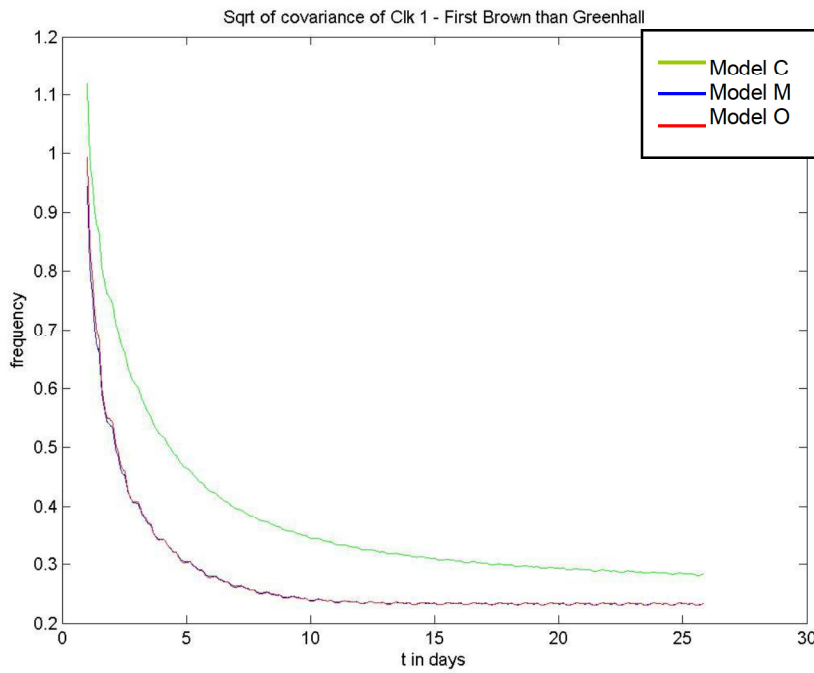


Figure 14. First Brown then Greenhall frequency covariance of clock 1, in units of ns/d.

CONCLUSIONS

Using a highly simplified model for the operational GPS Kalman Filter, it has been shown that the real-time positioning ability of GPS (PII) is insensitive to the improved ground clocks and composite clocks.

In contrast, GPS Time within the Kalman Filter would be more stable if all GPS sites had environmentally protected masers or the USNO-controlled sites had atomic fountains. Its stability can be additionally increased applying the Greenhall composite clock. The Greenhall composite clock shows the most promising results for each model.

Furthermore, a combination of both reduction methods is suggested to instead of running the Greenhall reduction alone. The clock estimates are unchanged, and the frequency and drift parts of the covariance are reduced. The improvement by applying both covariance reduction algorithms are reported as empirical here, but one of us (C. Greenhall) intends to publish a mathematical proof in the near future.

ACKNOWLEDGMENTS

We thank Benjamin Harris and the University of Texas for use of the GPS Toolkit, and Dr. Paul Koppang for a critical review of this paper. This research was carried out in part at the Jet Propulsion Laboratory, California Institute of Technology, under a contract with the National Aeronautics and Space Administration.

REFERENCES

- [1] <http://www.aero.org/education/primers/gps/elements.html>.
- [2] http://www.kowoma.de/en/gps/control_segment.htm.
- [3] D. Manning, 2009, "AF/NGA GPS Monitor Station High-Performance Cesium Frequency Standard Stability 2007/2008: From NGA Kalman Filter Clock Estimates," in Proceedings of the 40th Precise Time and Time Interval (PTTI) Systems and Applications Meeting, 1-4 December 2008, Reston, Virginia, USA (U.S. Naval Observatory, Washington, D.C.), pp. 335-348.
- [4] T. J. H. Craddock, R. J. Broderick, C. P. Petersen, and A. Hu, 2009, "The GPS Toolkit: Open Source Clock Tools." in Proceedings of the 40th Precise Time and Time Interval (PTTI) Systems and Applications Meeting, 1-4 December 2008, Reston, Virginia, USA (U.S. Naval Observatory, Washington, D.C.), pp. 255-273.
- [5] C. Zucca and P. Tavella, 2005, "The clock model and its relationship with the Allan and related variances," **IEEE Transactions on Ultrasonics, Ferroelectrics, and Frequency Control**, UFFC-52, 289-296.
- [6] J. W. Chaffee, 1987, "Relating the Allan Variance to the Diffusion Coefficients of a Linear Stochastic Differential Equation Model for Precision Oscillators," **IEEE Transactions on Ultrasonics, Ferroelectrics, and Frequency Control**, UFFC-34, 655-658.

- [7] K. R. Brown, 1991, "*The theory of the GPS composite clock,*" in Proceedings of the ION GPS-91, 11-13 September 1991, Albuquerque, New Mexico, USA (Institute of Navigation, Alexandria, Virginia), pp. 223-242.
- [8] C. A. Greenhall, 2007, "*A Kalman filter clock ensemble algorithm that admits measurement noise,*" **Metrologia**, **43**, S311-S321.
- [9] J. A. Davis, C. A. Greenhall, and P. W. Stacey, 2005, "*A Kalman filter clock algorithm for use in the presence of flicker frequency modulation noise,*" **Metrologia**, **42**, 1-10.